# Observations of a Submesoscale Cyclonic Filament in the Marginal Ice Zone

**Wilken-Jon von Appen**[1] [ID], **Claudia Wekerle**[1] [ID], **Laura Hehemann**[1], **Vibe Schourup-Kristensen**[1] [ID], **Christian Konrad**[1,2] [ID], and **Morten H. Iversen**[1,2] [ID]

[1] Alfred Wegener Institute, Helmholtz Centre for Polar and Marine Research, Bremerhaven, Germany, [2] MARUM and Faculty of Geosciences, University of Bremen, Bremen, Germany

**Abstract** Submesoscale flows are energetic motions on scales of several kilometers that may lead to substantial vertical motions. Here we present satellite and ship radar as well as underway conductivity-temperature-depth and Acoustic Doppler Current Profiler observations of a cyclonic submesoscale filament in the marginal ice zone of Fram Strait. The filament created a 500-m thin and 50-km long sea ice streak and extends to >250-m depth with a negative/positive density anomaly within/below the halocline. The frontal jets of 0.5 m/s are in turbulent thermal wind balance while the ageostrophic secondary circulation in places appears to subduct Atlantic Water at >50 m/day. Our study reveals the submesoscale dynamics related to sea ice shapes that can be sensed remotely and shows how submesoscale dynamics contribute to shaping the marginal ice zone. It also demonstrates the co-occurrence and mixing of water masses over short horizontal scales, which has implications for ocean and sea ice models and understanding of patch formation of planktonic organisms.

**Plain Language Summary** A sea ice streak in the marginal ice zone was observed with radar measurements. Below this streak in situ shipboard measurements of the temperature, salinity, and velocity field revealed a cyclonic submesoscale filament. This is a line of denser water of a few kilometers width bounded by strong counteracting velocities. This denser water is also associated with a different water mass and thus a change in biological properties and communities. This provides in situ confirmation for previous theoretical conclusions of how oceanic flows on kilometer scales structure the sea ice and biology in the marginal ice zone. The understanding of such small-scale processes helps improve computer models of the ocean and sea ice dynamics. It also makes it possible to interpret oceanic flows from remote sensing of sea ice. Furthermore, it gives indication over which horizontal scales biological processes vary in the ocean.

## 1. Introduction

Relatively warm and salty Atlantic Water (AW) from lower latitudes enters Fram Strait, between Svalbard and Greenland, where it interacts with cold and fresh Polar Water (PW) from the Arctic Ocean. The eastern Fram Strait is the last location where AW is subject to atmospheric cooling and densification before it gets subducted below PW in central Fram Strait. Subsequently, it is transported southward in the East Greenland Current (Figure 1a) toward Denmark Strait (Håvik et al., 2017). There it is a major source of the overflow water that becomes North Atlantic Deep Water (Dickson & Brown, 1994) and contributes to the Atlantic Meridional Overturning Circulation. Hattermann et al. (2016) suggested that the subduction in Fram Strait is due to baroclinic instability of the near surface density gradient between AW and PW or due to mesoscale eddies that are shed from the West Spitsbergen Current (WSC; Figure 1a). Mesoscale-resolving simulations of Fram Strait (Hattermann et al., 2016; Wekerle et al., 2017) demonstrate that convergent flow between mesoscale eddies commonly occurs in central Fram Strait. The relative vorticity frequently exceeds $\pm0.5f$ in the simulations that permit, but not fully resolve, submesoscale flows. Furthermore, northward flowing warm AW and southward flowing cold and sea ice laden PW create a semipermanent sea ice edge in Fram Strait (von Appen et al., 2016). This is different from the large, seasonal latitudinal excursion of the sea ice edge that is common for the rest of the Arctic and Antarctic. The width of the marginal ice zone (MIZ) in the Arctic during summer has increased by ≈40% during the past decades (Strong & Rigor, 2013) and is expected to continue to occupy larger areas. Already >30-years ago, it was realized that the shape and pathways of sea ice in the MIZ of Fram Strait are
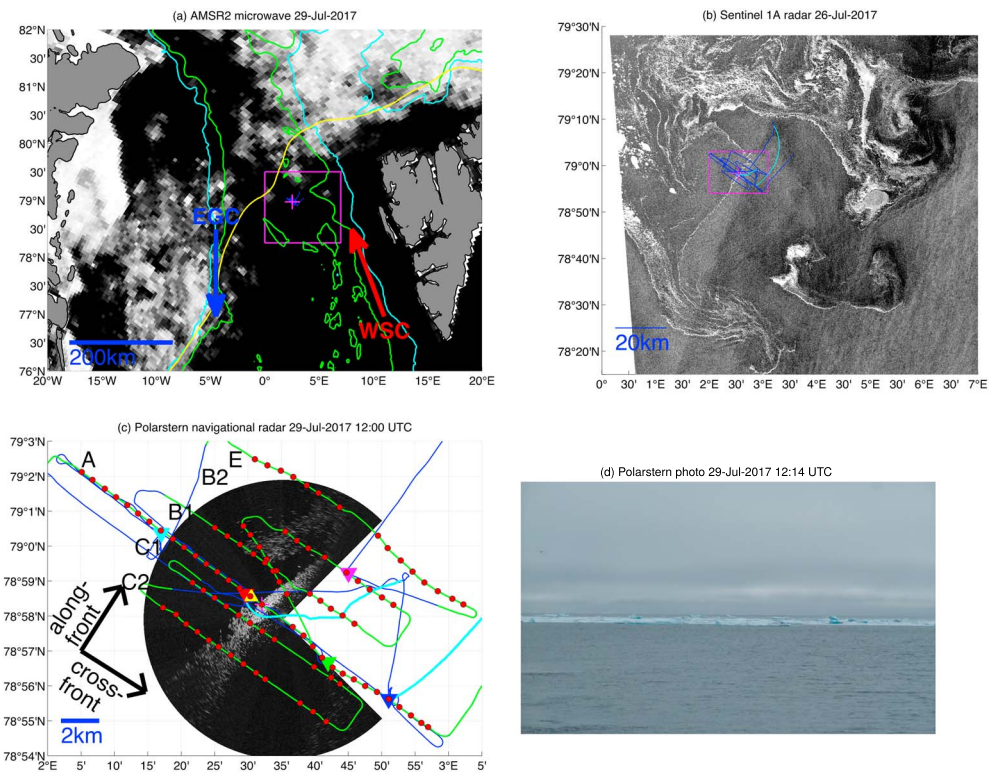
**Figure 1.** Sea ice distribution in the study area (black = open water, white = sea ice). (a) AMSR2 microwave sea ice concentration on 29 July 2017, (b) Sentinel 1A (©European Space Agency) radar reflectivity on 26 July 2017, (c) RV *Polarstern* navigational radar reflectivity on 29 July 2017 12:00 UTC approaching the ice streak, (d) photo taken from yellow location in Figure 1c on 29 July 2017 12:14 UTC looking back at the ice streak after the first crossing. The magenta boxes in Figures 1a and 1b correspond to the domain of Figures 1b and 1c and the magenta "+" in Figures 1a–1c marks the ($x = 0$ km, $y = 0$ km) location used in Figure 2/SI05. The yellow line in Figure 1a is the 50% contour of the 2002–2017 time mean sea ice concentration, and the cyan/green lines are the 1,000-/2,000-m isobaths. The rough locations of the West Spitsbergen Current (WSC) and East Greenland Current (EGC) are sketched. The blue line in Figure 1b/1c is the ship track with the green part in Figure 1c, the part where VMADCP data are used. The cyan lines in Figure 1b/1c are the drifting sediment track trajectories. The red dots in Figure 1c are the UCTD profile locations with transect names indicated in the top left. The colored triangles are the locations of the CTD profiles. AMSR2 = Advanced Microwave Scanning Radiometer-2. ADCP = Acoustic Doppler Current Profiler; VMADCP = Vessel-mounted ADCP; CTD = conductivity-temperature-depth, UCTD = underway CTD.

dictated by oceanic motion (Johannessen et al., 1987; Shuchman et al., 1987) potentially related to bathymetric features.

Submesoscale fronts are ubiquitous in the ocean (e.g., Adams et al., 2017; Ramachandran et al., 2018; Thomas et al., 2013) where strong horizontal density gradients are created in the upper ocean such as in the MIZ. However, much of our knowledge of submesoscale dynamics is based on theoretical considerations and numerical simulations as the small scale of the dynamics poses observational challenges. For outcropping isopycnals at the surface, McWilliams et al. (2009) sketched the theoretical qualitative flow field in a "dense filament," which can be thought of as two parallel fronts between light-dense and dense-light water at the surface. The flow field is composed of geostrophically balanced cyclonic frontal jets in the along-front direction and an ageostrophic (overturning) secondary circulation (ASC) in the cross-frontal plane. In the center of the filament, dense water is subducted by the ASC, while lighter water is raised on either side of the filament. The locations of dense filaments are presumed to correlate with the accumulation of surfactants at the sea surface since they are positively buoyant and are not subducted by the ASC (McWilliams et al., 2009). Numerical simulations also indicate that cyclonic eddies and filaments can efficiently trap sea ice (Manucharyan & Thompson, 2017). Sea ice, unlike surfactants, can be sensed remotely during windy conditions. Since a global understanding of submesoscale flow statistics is still lacking, this has led to attempts to infer the statistics in the MIZ from high-resolution sea ice imagery (Fajber et al., 2018).

Intense vertical velocities in submesoscale fronts and filaments have been linked to the resupply of nutrients to, as well as biomass export from, the euphotic layer (Klein & Lapeyre, 2009). Traditional physical and biological measurement campaigns are too coarse to capture the small spatial and temporal scales of the submesoscale. For example, the predicted spatial correlation between surfactants/sea ice and the center of dense (surface) filaments has not been observationally proven. A combination of multiple high-resolution measurement techniques is required to advance our knowledge of this nascent field with significant interdisciplinary ramifications. Recent observations of submesoscale processes in the open ocean are based on gliders (e.g., Thompson et al., 2016), satellite data (e.g., Buckingham et al., 2017), and intensive ship surveys (e.g., Klymak et al., 2016), but no in situ observations in the MIZ exist to date.

Here we present three-dimensional in situ observations of a cyclonic filament in the MIZ in Fram Strait. Based on an innovative combination of high-resolution measurement techniques, we show how the filament modifies the sea ice distribution and causes mixing.

## 2. Data and Methods

A Seabird 911+ conductivity-temperature-depth (CTD)-Rosette was used to obtain vertical profiles from 5-m to 500-m depth (Schewe & Rohardt, 2017). The CTD data from the whole cruise were processed using precruise and postcruise manufacturer calibrations and a comparison to bottle salinities that were measured on board with an Optimare Precision Salinometer. Chlorophyll fluorescence and oxygen saturation have not been in situ calibrated.

A Seabird Underway CTD (UCTD) was used in conjunction with an Oceanscience winch system on a Kevlar line in a tow-yo mode of operation that achieved downcast profiles with good data between 15 m and 210 m (von Appen, 2018). The UCTD was stored in a water bath with a few drops of Triton-X to keep the conductivity sensor wet prior to the initial profile of a transect. The UCTD is an unpumped system and the time delay between the temperature and conductivity sensors depends on the vertical drop speed that decreases during each downward profile. We used the processing procedure and empirical parameters of Ullman and Hebert (2014). Subsequently, the salinity profiles were low-pass filtered with a 4-m vertical cutoff. Since the underway CTD was last factory calibrated in March 2015, we removed a constant salinity offset of 0.01 from the UCTD data such that the maximum measured salinities from the CTD and UCTD agree. The density profiles were reordered in the vertical to remove density overturns that result from salinity spiking that the method of Ullman and Hebert (2014) can only partially remove.

A vessel-mounted 150-kHz RDI Ocean Surveyor Acoustic Doppler Current Profiler (VMADCP) recorded ocean velocities along the cruise track (Schewe & Witte, 2017); here we use the part of the track marked green in Figure 1c with a bin size of 4 m and a depth coverage between 17 and 250 m. The VMADCP data of the whole cruise were processed using the Matlab toolbox "ossi" of GEOMAR that implements the calibration of the misalignment angle between the Acoustic Doppler Current Profiler's transducers and the ship's forward direction. No detiding was performed, because the barotropic tidal amplitude in the deep (>2,000 m) Fram Strait is <0.03 m/s as determined from nearby mooring records (e.g., von Appen et al., 2016). Laplacian splines under tension (Smith & Wessel, 1990) were used to interpolate the individual UCTD profiles and the 1-min averaged VMADCP data onto a 500-m cross-frontal distance by 5-m vertical grid.

Sea ice concentration from microwave satellites Advanced Microwave Scanning Radiometer for Earth-Observing System (AMSRE) and Advanced Microwave Scanning Radiometer-2 (AMSR2) was downloaded from the University of Bremen: https://seaice.uni-bremen.de/start/data-archive/ (Spreen et al., 2008). The mean sea ice edge was defined as the 50% contour of the time mean (1 June 2002 to 31 December 2017) AMSRE/AMSR2 sea ice concentration. Sentinel 1A satellite synthetic aperture radar (SAR) reflectivity showing both small and large sea ice floes as well as internal waves was sent to RV *Polarstern* in near real time by Drift and Noise. Due to cloud cover, only an image from 26 July 2017 exists. Specular reflections and a linear 2-D gradient were removed in order to enhance the contrast between sea ice and water in all regions of the image. An OceanWaves sigma S6 WaMoS II system digitized the navigational radar of RV *Polarstern* with the range settings chosen such that the contrast between sea ice and open water was maximized.

A drifting sediment trap was equipped with a surface float with a Global Positioning System/Iridium connection sending its position every 2 min. Below was a Gleistein Geotwin 14-mm diameter nylon deep sea line of

400-m length and a 30-kg weight at the bottom. No calibration exists for how a drifting sediment trap maps the upper ocean flow field, but it is expected that it averages the top 400 m as the drag is distributed relatively uniformly over that depth range.

## 3. Results

### 3.1. Shape of the Ice Streak

There was extensive sea ice coverage northeast of 0°EW/80°N during late July 2017 while the remainder of Fram Strait had very low ice concentration (Figure 1a). The region southeast of the year-round mean sea ice edge and west of the northward warm water flow of the WSC featured a highly complex shape of the MIZ (Figure 1b). Radar reflectivity on 26 July 2017 showed a nearly straight streak of sea ice with a northeast-southwest extent of ≈50 km and a width of only 500 m. The in situ observations described below show that this was due to a cyclonic filament. At the northeast end of the streak, the ice streak made a ≈ 90° corner and extended in a less straight and compacted manner to the northwest.

The linear shape of the ice streak, the strong contrast between open water on either side of the ≈500 m wide streak, and the nearly 100% sea ice concentration inside is confirmed by RV *Polarstern*'s navigational radar (Figure 1c) and is also visually apparent (Figure 1d). The typical size of the individual floes was ≈10−50 m, and they were actively melted by the ocean water. It was also visible that the aggregation was tighter (with a tighter transition from 0% to 100% ice concentration) on the northwestern side of the streak than on the southeastern side.

On 29 July 2017, the long UCTD/VMADCP Transect A crossed the filament from 12-km southeast to 12-km northwest of the largest ice concentration with a UCTD profile every ≈700 m in the cross-frontal direction. Near the ice, the UCTD profiling had to be interrupted for 2 km (Figure 2a). Subsequently, the five parallel Transects B1, B2, C1, C2, and E (cruise track in Figure 1c, data shown in Figure SI05 in the supporting information) focussed on the area ±4 km around the filament in order to establish the along-front structure at a resolution of ≈2 km. Due to the limited battery capacity of the UCTD, the transects were interspersed with stations (colored triangles in Figure 1c) for CTD and other profiling equipment. The survey took >1.5 days or roughly 3 inertial periods.

### 3.2. Density and Velocity Structure of the Filament

The upper 50 m of the water column is salinity stratified with salinities increasing from <32 to >34.8. Below this highly stratified freshwater layer, the water column is temperature stratified. Near the ice streak (larger spacing between consecutive UCTD profiles in Figure 2a/SI05a corresponding to cross-front distance $x$=0 km), there is colder ($\approx$ 1.5°C) water below 150 m while on either side of the ice streak, the water is $> 3.5$°C. This causes a strong density contrast with water $>27.95$ kg/m$^3$ near $x$=0 km in Transects A and B, while even water $<27.9$ kg/m$^3$ is absent in the top 210 m $>8$ km from the center. The 27 kg/m$^3$ isopycnal is shallower (<15 m) on either side of the filament and depressed (≈25 m) near the center. This results in a much higher stratification at ≈80 m depth near the center than on either side of the filament. In the lower halocline, an intermediate temperature maximum $> 5$°C (indicative of AW) is present near the center, while some profiles on either side exhibit intermediate temperature minima of $\approx -1$ °C (indicative of PW).

The parallel sections (Figure SI05) confirm that the aspect ratio (along-front scale to cross-front scale) of the filament is not 1 (which would correspond to an eddy), but that it is significantly elongated with at least an aspect ratio of 5 at the time of the survey. Note that the SAR image 3 days earlier (Figure 1b) points to an even larger aspect ratio. A mean cross-front (southeastward) velocity $u$ of 0.1 m/s (as measured by the VMADCP and subtracted from Figure 2b/SI05b) leads to a translation of the system and may account for the apparent motion of the center of the filament from $x = 0-2$ km in Transects A and B to $x = 2-4$ km in Transect C.

The along-front velocity $v$ (Figure 2b) shows a clear signature of cyclonic frontal jets as expected for a dense filament (McWilliams et al., 2009). The velocities are enhanced near $x = \pm 3$ km and in 50- to 100-m depth with the maximum exceeding 0.5 m/s. The zero crossing of the along-front velocity coincides with the shallowest depths of the 27.9 and 27.95 kg/m$^3$ isopycnals. However, there is also a significant barotropic component to the frontal jets that extends below the range of the VMADCP observations. The deeper CTD profiles show that the increased density in the center of the filament extends to >400 m (Figure 3a). Using the maximum velocities to estimate the relative cyclonic vorticity yields $\zeta = \frac{\Delta v}{\Delta x} \approx \frac{0.5 \text{m/s}}{3,000 \text{m}} \approx 0.9 f$. That is, the Rossby number $Ro = \frac{\zeta}{f}$ is order 1 and the filament clearly has a submesoscale character with a significant ageostrophic flow.
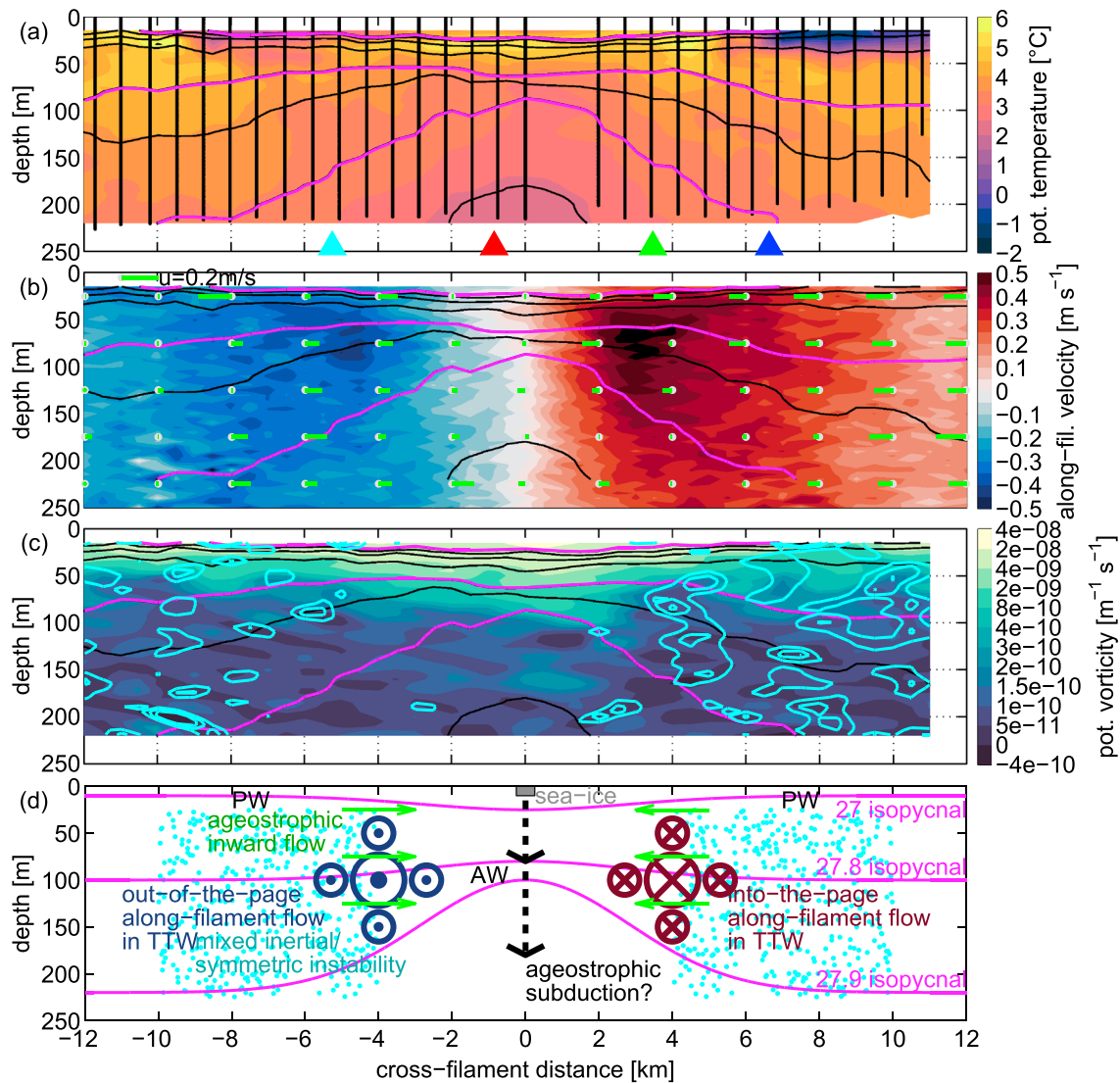
**Figure 2.** Section along Transect A. (a) Potential temperature with potential density overlain (27, 27.8, 27.9 kg/m$^3$ in magenta, 26, 27.2, 27.4, 27.6, 27.85, 27.95 in black). The UCTD profiles are indicated by the black vertical lines. The colored triangles are the locations of the CTD profiles. (b) Along-filament velocity (positive = northeastward and into the page). The cross-frontal velocity (a constant of 0.1 m/s has been subtracted) is shown as green lines with a 0.2 m/s scale bar in the top left corner. (c) Ertel potential vorticity with the 10°/20°/30° contours of $\phi_{Ri_B}$-$\phi_C$ overlain in cyan; elsewhere $\phi_{Ri_B}$-$\phi_C > 30°$. (d) Schematic of the observed filament structure. CTD = conductivity-temperature-depth; AW = Atlantic Water; PW = Polar Water.

### 3.3. Ageostrophic Circulation

The along-front circulation is not in simple geostrophic thermal wind balance with the observed density field. Rather, the vertical shear of the VMADCP velocities accounts for only ≈60% of the thermal wind shear from the density observations. This suggests that the frontal jets are in turbulent thermal wind balance (Gula et al., 2014), that is, isopycnal and diapycnal mixing of horizontal momentum in the region of the frontal jets partially balances the thermal wind shear and reduces the observed $\frac{\partial v}{\partial z}$.

The Ertel potential vorticity (PV) is defined as $\Pi = \frac{1}{g}\left(f\frac{\partial b}{\partial z} + \frac{\partial v}{\partial x}\frac{\partial b}{\partial z} - \frac{\partial v}{\partial z}\frac{\partial b}{\partial x}\right)$ where $g$ is the acceleration due to gravity and $b = -g\frac{\rho}{\rho_0}$ is the buoyancy. Note that the tilting vorticity (last term in $\Pi$) is often (e.g., Haine & Marshall, 1998; Thomas et al., 2013) recast assuming the flow is in simple thermal wind balance. Since this is not the case here, it would lead to $\Pi \ll 0$ or $\Pi \gg 0$ depending on whether $\frac{\partial v}{\partial z}$ or $\frac{\partial b}{\partial x}$ is substituted by the other one. In fact the observed Ertel PV along Transect A (Figure 2c) is slightly larger than 0 for $|x| > 4$ km and below the halocline. In the center of the filament, between the frontal jets, the relative vorticity is positive (cyclonic) and brings the Ertel PV to values above 0 indicating that the flow may be stable there to small-scale instabilities. By
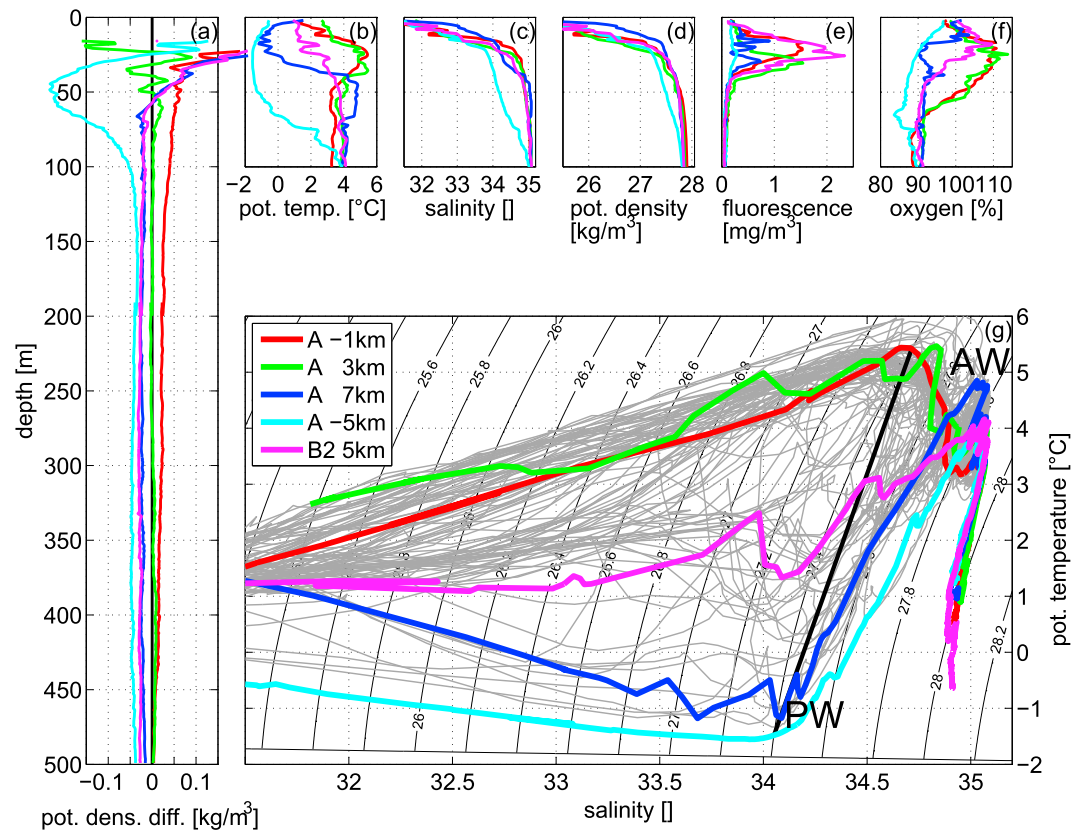
**Figure 3.** CTD profiles (colors as in Figure 1c/2a/SI05a). Panel (a) shows potential density difference between the respective CTD profile and the mean of the five profiles at each depth. The UCTD profiles are gray in (g). Atlantic Water (AW) and Polar Water (PW) are marked black in (g) as is their mixing line. CTD = conductivity-temperature-depth.

contrast, on the rim of the filament, the anticyclonic vorticity together with the tilting term reduces the Ertel PV to values near (and sometimes below) 0. Submesoscale instabilities will bring the flow back to marginal stability, which is a PV of 0, therefore, negative values of PV are not expected to be observed. Thomas et al. (2013) recast the ratio of the geostrophic shear to the stratification as angle $\phi_{Ri_B}$ and the Rossby number as angle $\phi_C$. When $\phi_{Ri_B} - \phi_C$ approaches 0, which happens in the regions of anticyclonic vorticity, mixed inertial/symmetric instability occurs. This instability extracts energy from both the lateral and the vertical velocity shear. Likely, this reduces the gradients and causes horizontal and vertical mixing at the rim of the filament consistent with the observation of turbulent thermal wind. Conversely, the cyclonic shear in the center of the filament appears to suppress symmetric instability and acts to stabilize the flow structure.

The cross-front velocity (Figure 2b/SI05b) shows inward motion of up to 0.1 m/s on either side of the filament in Transects A and B. The signature in Transect C is more ambiguous and there was fast (>0.25 m/s) southeastward flow in Transect E. Transect E is outside of the linear segment of the ice streak and instead at the location where it continues at a $\approx$ 90° angle northwestward (Figure 1b). The flow of Transect E in Figure SI05b may thus rather be the along-front flow of a northwestward oriented filament.

The convergent cross-front flow likely accumulates the sea ice and increases the freshwater layer thickness (depressed 27 kg/m$^3$-isopycnal). The convergent cross-front flow indicates subduction. In order to obtain the order of magnitude of the subduction, we make the following assumptions: An inward flow of $u = 0.05$ m/s occurs over a depth of $d = 100$ m on either side of a cross-frontal width of $l = 8,000$ m. Then the vertical velocity is $w = 2*u*\frac{d}{l} = 0.0013$ m/s = 108 m/day or 72 m in 16 hr. As an alternative way to estimate the order of magnitude of $w$, if we consider the survey as sampling an along-front uniform structure over different points in time and not as a synoptic snapshot mapping spatial variability (note that the survey likely captures both temporal and spatial variability), then the observations indicate that in the time from Transect A to Transect C1 of 16 hr, the 27.9 (27.925) kg/m$^3$ moved down by 50 (90) m. This is the same order of magnitude (100 m/day) as determined from the simple scaling above. Thus, our observations are kinematically consistent with the

circulation at an outcropping dense filament (e.g., McWilliams et al., 2009) even though the front was not at the ocean surface but rather below a strong halocline. Another way to estimate the vertical velocity is to solve the $\omega$ equation (Rudnick, 1996). However, the resulting patterns are highly sensitive to the precise numerical initial conditions (e.g., Garabato et al., 2001) and the survey took too long to synoptically resolve the velocity and density in 3-D. (Ship-powered towed profiling systems can complete a similar survey in $\approx$8 hr that might be sufficiently synoptic.) Therefore, our calculations with the $\omega$-equation method could only confirm the $\approx$100 m/day order of magnitude of the vertical velocity but not reveal further spatial patterns.

Central Fram Strait ($\approx$2,500-m water depth) is far away from the boundary currents that flow along the continental slopes. Therefore, direct topographic effects forcing the filament can be ruled out. Significant wind would represent a downfront wind forcing for one of the constituent fronts of the filament and upfront forcing for the other. Different from the observations, this would result in an asymmetric shape of the filament throughout the water column (note that only the sea ice streak showed slightly tighter aggegation on its northwestern side). The wind as measured by the meteorological station on board RV *Polarstern* was northerly at 8 m/s on 28 July 2017 and decreased from northerly at 5 m/s on 29 July 2017 to westerly at 3 m/s on 30 July 2017. Surface waves were dampened by isolated patches of sea ice seaward of the observation area further reducing the wind drag on the ocean underneath. Therefore, the wind forcing of the observed system was weak, which is reflected in the symmetric shape of the filament.

## 4. Discussion

A drifting sediment trap was deployed twice in order to reveal approximate Lagrangian barotropic trajectories. Deployment 1 (near the center of the filament; Figure 1c) traversed 8 km along a fairly jagged course in 18 h, which is equivalent to an average speed of $\approx$ 0.1 m/s. Conversely, deployment 2 (near the northeastward frontal jet; Figure 1b) traversed 26 km in 21 hr ($\approx$ 0.35 m/s) along a smooth path. This fast translation emphasizes the huge scale and large region of impact of the circulation associated with the filament. The filament thus appears to be associated with a fast long-range property transport that is not solely due to a uniform background flow as the two trajectories would have behaved more similarly otherwise. From a Lagrangian perspective, water parcels may only have short residence times of order 1 to a few days in the filament even though, from a Eulerian perspective, the filament appears to have moved little in the 3 days between the satellite image and our survey.

Biological sampling (data not shown) demonstrated that Atlantic and Polar species are in close proximity at the filament. At the interface between AW and PW, a CTD profile (magenta in Figure 3) along with 15 UCTD profiles shows the result of the isopycnal mixing (related to the instability and the turbulent thermal wind balance) between the two water masses with frequent occurrences of interleaving (Figure 3g). Notably, the mixed water had the highest chlorophyll fluorescence in the deep chlorophyll maximum (Figure 3e). The PW was likely nutrient deplete and thus low in phytoplankton standing stock. Conversely, AW showed oxygen supersaturation indicative of past primary production below the surface mixed layer (Figure 3f). The cyclonic filament also impressively demonstrates the short horizontal scales over which distinct and unmixed water masses co-occur. To the extent that biology acts as a passive tracer, it would change over the same short horizontal scales. Patch formation (Prairie et al., 2012) is still an unsolved but important problem in marine biology. Fronts are known to relate to patches of phytoplankton (Wulff et al., 2016), zooplankton (Trudnowska et al., 2016), and marine birds and mammals (Joiris & Falck, 2011) in Fram Strait. The CTD casts suggest that the submesoscale filament may have a similar structuring ability on biomass and nutrient distributions as well as biological communities.

Due to cabbeling, the mixture of two water masses with the same density has a higher density. For the mixture of the warmest AW core water and the coldest PW core water observed here, the density increases by 0.08 kg/m$^3$ (black line in Figure 3g). The mixing increases entropy, destroying the information about the regionally distinct surface forcing mechanisms, and releases available potential energy. This process likely increases the rate of subduction at the filament (Thomas & Shakespeare, 2015).

The mixing can also be considered to be between highly stratified AW and weakly stratified water. In the center of the filament, the high stratification is reminiscent of the temperature stratified summer conditions in the WSC. On the sides, the weak stratification may be related to winter conditions in the WSC or to Arctic AW outflow from the Arctic Ocean. The structure of the filament observed here is qualitatively different from a dense filament (e.g., McWilliams et al., 2009) in that the dense isopycnals of the filament do not outcrop near

the center of the filament. In contrast, the halocline above is a low salinity/low density layer on top that actually gets accumulated near the center of the filament. Therefore, the term "cyclonic filament" appears more appropriate than "dense filament." This study confirms that cyclonic filaments, even in the absence of outcropping isopycnals, accumulate positively buoyant material (sea ice in this case and surfactants more generally), which makes them visible with remote sensing techniques. However, in the MIZ, there may be an additional dynamic feedback whereby the accumulated sea ice melts (the surface water temperature was >-1°C in the ice field) and thereby releases additional freshwater to the ocean. This effect would further increase the freshwater accumulation in the upper ocean near the filament's center. Different from Manucharyan and Thompson (2017), the high velocities of the filament extend significantly deeper (≈50 m in Manucharyan & Thompson, 2017 versus >250 m here). Meltwater generates shallow horizontal density gradients, whereas the contrast between AW and PW leads to deep reaching horizontal density gradients. Since the filament presented here is rather deep reaching (its density anomaly extends to ≈400 m; Figure 3a), its structure may be specific to Fram Strait and the southern Eurasian Basin where AW and PW meet.

Fronts similar to the one shown here appear to lead to large velocities (>0.3 m/s) in the upper ocean for a duration of several days, likely often accompanied by later flow reversals if the opposite frontal jet passes over the particular location. Such flows are common in moored time series in central Fram Strait such as at mooring F6 (presented in von Appen et al., 2016) 50-km east of the observed cyclonic filament. The mooring record shows such events to be more frequent in fall to spring, possibly due to an increased rate of mesocale instability of the WSC then (von Appen et al., 2016). Likewise, numerical simulations show several filaments in central Fram Strait at all times, but their number and relative vorticity is smaller in summer (Wekerle et al., 2017).

Sea ice eddies (like the dipole in the southeast of Figure 1b) are prevalent in SAR images with typically ≈30 distinct features identifiable per month in the Fram Strait area (78–80°N) (Bondevik, 2011). Sea ice streaks are common in a 100-km radius around the location of this study with ≈5 distinguishable in the very intermittent satellite radar record of August 2017. Later during the cruise, a single UCTD/VMADCP transect crossed one of those ice streaks, revealing a qualitatively similar filamentary structure.

## 5. Conclusions

The submesoscale filament described here with its dynamics driven from below the halocline has a number of implications. Classically, the sea ice edge in the MIZ is thought of as a straight line that is advected over warmer water where the sea ice melts uniformly. In contrast, submesoscale flows may accumulate sea ice near warm water far into the MIZ and thereby substantially increase heat transport to the sea ice and thus melt rates. The appropriate energetic representation in ocean and sea ice models may not be achieved if they cannot resolve the submesoscale dynamics. Thus, the shape of the sea ice in the MIZ and the heat transport toward the sea ice may be fundamentally misrepresented. The downwelling in the filament may be an important mechanism exporting biomass (and thus carbon) from the euphotic zone. Conversely, the upwelling associated with the ageostrophic flow may (re)supply nutrients to the euphotic layer (Klein & Lapeyre, 2009).

The presence of AW at shallow depth is typical of Fram Strait but appears to spread into the Eurasian Basin of the Arctic Ocean (Polyakov et al., 2017, observed this "Atlantification"). Thus, the dynamics of deep reaching subsurface cyclonic filaments described here may become more important in larger areas of the future Arctic Ocean.

## References

Adams, K. A., Hosegood, P., Taylor, J. R., Sallée, J.-B., Bachman, S., Torres, R., & Stamper, M. (2017). Frontal circulation and submesoscale variability during the formation of a Southern Ocean mesoscale eddy. *Journal of Physical Oceanography*, *47*(7), 1737–1753.

Bondevik, E. (2011). Studies of eddies in the marginal ice zone along the East Greenland current using spaceborne synthetic aperture radar (SAR) (Master's thesis), University of Bergen.

Buckingham, C. E., Khaleel, Z., Lazar, A., Martin, A. P., Allen, J. T., Naveira Garabato, A. C., et al. (2017). Testing Munk's hypothesis for submesoscale eddy generation using observations in the North Atlantic. *Journal of Geophysical Research: Oceans*, *122*, 6725–6745. https://doi.org/10.1002/2017JC012910

Dickson, R., & Brown, J. (1994). The production of North Atlantic Deep Water: Sources, rates, and pathways. *Journal of Geophysical Research*, *99*(C6), 12,319–12,341.

Fajber, R., Manucharyan, G., & Wells, A. (2018). Signatures of submesoscale ocean flows in sea ice patterns in marginal ice zones. In *Ocean Sciences Meeting*. Portland, OR.

Garabato, A. C. N., Leach, H., Allen, J. T., Pollard, R. T., & Strass, V. H. (2001). Mesoscale subduction at the Antarctic polar front driven by baroclinic instability. *Journal of Physical Oceanography*, *31*(8), 2087–2107.

Gula, J., Molemaker, M. J., & McWilliams, J. C. (2014). Submesoscale cold filaments in the Gulf Stream. *Journal of Physical Oceanography*, *44*(10), 2617–2643.

Håvik, L., Pickart, R., Våge, K., Torres, D., Thurnherr, A., Beszczynska-Möller, A., et al. (2017). Evolution of the East Greenland current from Fram Strait to Denmark Strait: Synoptic measurements from summer 2012. *Journal of Geophysical Research: Oceans*, *122*, 1–21. https://doi.org/10.1002/2016JC012228

Haine, T., & Marshall, J. (1998). Gravitational, symmetric, and baroclinic instability of the ocean mixed layer. *Journal of Physical Oceanography*, *28*(4), 634–658.

Hattermann, T., Isachsen, P. E., von Appen, W.-J., Albretsen, J., & Sundfjord, A. (2016). Eddy-driven recirculation of Atlantic water in Fram Strait. *Geophysical Research Letters*, *43*, 1–9. https://doi.org/10.1002/2016GL068323

Johannessen, O., Johannessen, J., Svendsen, E., Shuchman, R., Campbell, W., & Josberger, E. (1987). Ice-edge eddies in the Fram Strait marginal ice zone. *Science*, *236*(4800), 427–429.

Joiris, C. R., & Falck, E. (2011). Summer at-sea distribution of little auks Alle alle and harp seals Pagophilus (Phoca) groenlandica in the Fram Strait and the Greenland Sea: Impact of small-scale hydrological events. *Polar Biology*, *34*(4), 541–548.

Klein, P., & Lapeyre, G. (2009). The oceanic vertical pump induced by mesoscale and submesoscale turbulence. *Annual Review of Marine Science*, *1*, 351–375.

Klymak, J. M., Shearman, R. K., Gula, J., Lee, C. M., D'Asaro, E. A., Thomas, L. N., et al. (2016). Submesoscale streamers exchange water on the north wall of the Gulf Stream. *Geophysical Research Letters*, *43*, 1226–1233. https://doi.org/10.1002/2015GL067152

Manucharyan, G., & Thompson, A. F. (2017). Submesoscale sea ice-ocean interactions in marginal ice zones. *Journal of Geophysical Research: Oceans*, *122*, 9455–9475. https://doi.org/10.1002/2017JC012895

McWilliams, J., Colas, F., & Molemaker, M. (2009). Cold filamentary intensification and oceanic surface convergence lines. *Geophysical Research Letters*, *36*, L18602. https://doi.org/10.1029/2009GL039402

Polyakov, I. V., Pnyushkov, A. V., Alkire, M. B., Ashik, I. M., Baumann, T. M., Carmack, E. C., et al. (2017). Greater role for Atlantic inflows on sea-ice loss in the Eurasian basin of the Arctic Ocean. *Science*, *356*(6335), 285–291.

Prairie, J. C., Sutherland, K. R., Nickols, K. J., & Kaltenberg, A. M. (2012). Biophysical interactions in the plankton: A cross-scale review. *Limnology and Oceanography: Fluids and Environments*, *2*(1), 121–145.

Ramachandran, S., Tandon, A., Mackinnon, J., Lucas, A., Pinkel, R., Waterhouse, A., et al. (2018). Submesoscale processes at shallow, salinity fronts in the Bay of Bengal: Observations during the winter monsoon. *Journal of Physical Oceanography*, *48*(3), 479–509. https://doi.org/10.1175/JPO-D-16-0283.1

Rudnick, D. L. (1996). Intensive surveys of the Azores front: 2. Inferring the geostrophic and vertical velocity fields. *Journal of Geophysical Research*, *101*(C7), 16,291–16,303.

Schewe, I., & Rohardt, G. (2017). CTD raw data files from POLARSTERN cruise PS107, link to tar-archive. *PANGAEA*. https://doi.org/10.1594/PANGAEA.883364

Schewe, I., & Witte, H. (2017). Raw data of continuous VM-ADCP (vessel-mounted Acoustic Doppler Current Profiler) profile during POLARSTERN cruise PS107 (ARK-XXXI/2). *PANGAEA*. https://doi.org/10.1594/PANGAEA.883356

Shuchman, R., Burns, B., Johannessen, O., Josberger, E., Campbell, W., Manley, T., & Lannelongue, N. (1987). Remote sensing of the Fram Strait marginal ice zone. *Science*, *236*(4800), 429–431.

Smith, W., & Wessel, P. (1990). Gridding with continuous curvature splines in tension. *Geophysics*, *55*, 293–305.

Spreen, G., Kaleschke, L., & Heygster, G. (2008). Sea ice remote sensing using AMSR-E 89-GHz channels. *Journal of Geophysical Research*, *113*, C02S03. https://doi.org/10.1029/2005JC003384

Strong, C., & Rigor, I. G. (2013). Arctic marginal ice zone trending wider in summer and narrower in winter. *Geophysical Research Letters*, *40*, 4864–4868. https://doi.org/10.1002/grl.50928

Thomas, L. N., & Shakespeare, C. J. (2015). A new mechanism for mode water formation involving cabbeling and frontogenetic strain at thermohaline fronts. *Journal of Physical Oceanography*, *45*(9), 2444–2456.

Thomas, L. N., Taylor, J. R., Ferrari, R., & Joyce, T. M. (2013). Symmetric instability in the Gulf Stream. *Deep Sea Research Part II: Topical Studies in Oceanography*, *91*, 96–110.

Thompson, A. F., Lazar, A., Buckingham, C., Naveira Garabato, A. C., Damerell, G. M., & Heywood, K. J. (2016). Open-ocean submesoscale motions: A full seasonal cycle of mixed layer instabilities from gliders. *Journal of Physical Oceanography*, *46*(4), 1285–1307.

Trudnowska, E., Gluchowska, M., Beszczynska-Möller, A., Blachowiak-Samolyk, K., & Kwasniewski, S. (2016). Plankton patchiness in the Polar Front region of the West Spitsbergen Shelf. *Marine Ecology Progress Series*, *560*, 1–18.

Ullman, D. S., & Hebert, D. (2014). Processing of underway CTD data. *Journal of Atmospheric and Oceanic Technology*, *31*(4), 984–998.

von Appen, W.-J. (2018). Underway CTD raw data collected during POLARSTERN cruise PS107. *PANGAEA*. https://doi.org/10.1594/PANGAEA.886146

von Appen, W.-J., Schauer, U., Hattermann, T., & Beszczynska-Möller, A. (2016). Seasonal cycle of mesoscale instability of the West Spitsbergen Current. *Journal of Physical Oceanography*, *46*(4), 1231–1254. https://doi.org/10.1175/JPO-D-15-0184.1

Wekerle, C., Wang, Q., von Appen, W.-J., Danilov, S., Schourup-Kristensen, V., & Jung, T. (2017). Eddy-resolving simulation of the Atlantic water circulation in the Fram strait with focus on the seasonal cycle. *Journal of Geophysical Research: Oceans*, *122*, 8385–8405. https://doi.org/10.1002/2017JC012974

Wulff, T., Bauerfeind, E., & von Appen, W.-J. (2016). Physical and ecological processes at a moving ice edge in the Fram Strait as observed with an AUV. *Deep Sea Research*, *115*, 253–264. https://doi.org/10.1016/j.dsr.2016.07.001